Structural Engineering and Mechanics, *Vol. 58, No. 2 (2016) 301-326*
DOI: http://dx.doi.org/10.12989/sem.2016.58.2.301

New optimization method of patch shape to improve the effectiveness of cracked plates repair

Mohamed S. Bouchiba* and Boualem Serier

Department of Mechanical Engineering, University of Sidi Bel Abbes, BP89 cité Arbi Ben M'Hidi, Sidi Bel Abbes 22 000, Algeria

(Received November 7, 2015, Revised January 13, 2016, Accepted January 26, 2016)

Abstract. An optimization method of patch shape was developed in this study, in order to improve repair of cracked plates. It aimed to minimize three objectives: stress intensity factor, patch volume and shear stresses in the adhesive film. The choice of these objectives ensures improving crack repair, gaining mass and enhancing the adhesion durability between the fractured plate and the composite patch. This was a multi-objective optimization combined with Finite elements calculations to find out the best distribution of patch height with respect to its width. The implementation of the method identified families of optimal shapes with specific geometric features around the crack tip and at the horizontal end of the patch. Considerable mass gain was achieved while improving the repair efficiency and keeping the adhesive shear stress at low levels.

Keywords: patch repair; stress intensity factor; adhesive shear; finite elements method; shape optimization

1. Introduction

Bonded repair of structural components is widely used in industry. It is preferred over other repair techniques such as riveted patches. This is because bonded composite patches give more conformance to complex components. They are, also, used without drilling holes and they bring better transfer loads through the adhesive (Baker *et al*. 2002, Baker *et al*. 2004).

Several studies were carried out to analyze this technique. Many researchers showed the effectiveness of boned patches in reducing Stress Intensity Factor SIF (Achour *et al*. 2003, Belhouari *et al*. 2004, Gu *et al*. 2011, Shiuh-Chuan and Chao 2011, Majid Jamal-Omidi *et al*. 2014, Mokadem *et al*. 2015). In addition to that, service life can be improved without replacing the cracked part. However, it is important to investigate the effects of repair parameters because bad design can be more dangerous (Tsai and Shen 2004).

Many researchers addressed the effects of geometric parameters on the repair effectiveness. Different shapes were considered. Rectangular, square, circular, octagonal, and oval shapes were all analyzed using Finite Elements Method FEM to asses the SIF reduction that can be obtained (Kumar and Hakeem 2000, Kaddouri *et al*. 2008, Ramji *et al*. 2013, Kashfuddoja and Ramji

*Corresponding author, M.Sc., E-mail: salaheddine.bouchiba@yahoo.fr

http://www.techno-press.org/?journal=sem&subpage=8 ISSN: 1225-4568 (Print), 1598-6217 (Online)

2014). These works brought out the positive effect of a smaller patch length perpendicular to the crack (Mahadesh Kumar and Hakeem 2000), and the effectiveness of an expanded rectangular patch in its parallel direction (Ramji *et al.* 2013, Kashfuddoja and Ramji 2014).

However, it was important to investigate irregular shapes to assess their effectiveness. Roberto Brighenti (2006, 2007) developed a genetic algorithm to find the best configuration for improving fractured sheets, and he found out a tringle-like shape developed over a crack tip. Mhamdia Rachid *et al.* (2012), on the other hand, used a rectangular patch and removed progressively some regions, and he ended up by finding out an arrow shape.

This paper leads more investigations about patch shapes but in a different way. It uses a probabilistic approach called "an Estimation Distribution Method EDM" to analyze the effect of material patch distribution over the cracked plate, and looks for the optimal distribution, which allows reaching three objectives:

- Reducing SIF
- Reducing patch volume
- Reducing adhesive shear stress in the adhesive film.

This is an iterative and metaheuristic process implemented through a combination of FEM and a multi-objective algorithm.

2. Problem definition and modelling description:

2.1 General description of the repaired plate geometry

The problem consists of performing a symmetric repair of a center-cracked plate made of aluminum alloy subjected to a uniaxial tensile loading. The half crack length is a=12 mm. An external composite patch is bonded to the plate over the damaged region, using an Epoxy adhesive. Half of the repaired plate geometry is shown in Fig. 1. The dimensions and the

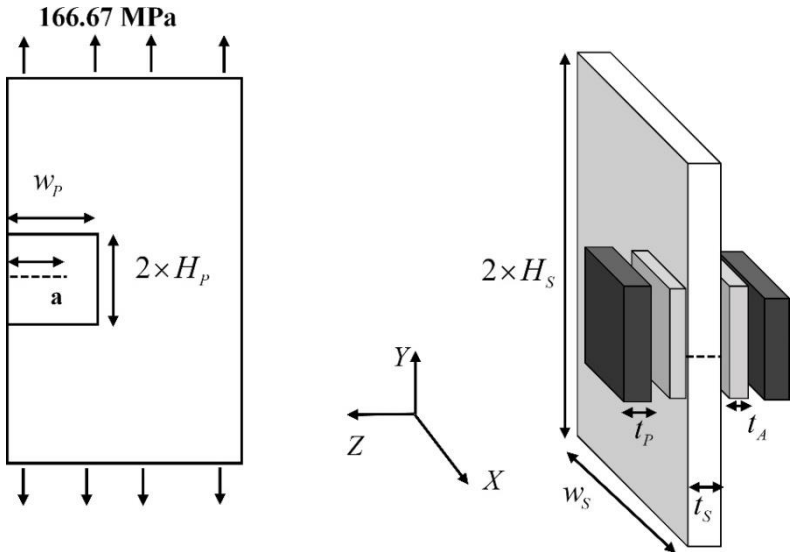

Fig. 1 General geometry of the repaired plate (one-half represented)

Table 1 Mechanical properties

	Composite patch	Aluminum plate	Adhesive
E_1 (GPa)	135	71.709	21.58E-01
E_2 (GPa)	9		
E_3 (GPa)	9		
G_{13} (GPa)	5		
G_{12} (GPa)	5		
G_{23} (GPa)	8		
υ_{12}	0.3	0.33	0.35
υ_{13}	0.3		
υ_{23}	0.02		
τ_l (MPa) adhesive linear limit shear stress			27.43

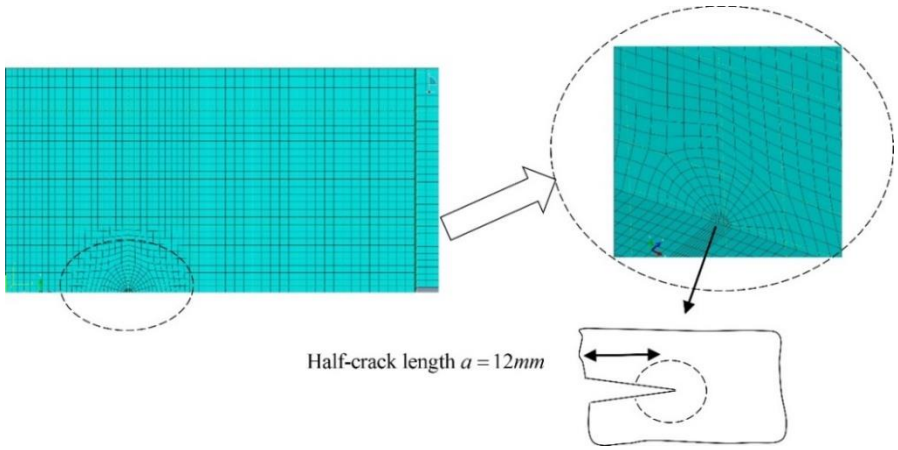

Fig. 2 Finite elements meshing at the crack region

mechanical properties are taken from the study of Mahadesh Kumar and Hakeem (2000). The sheet has the total width $2\times w_s$=240 mm and total height $2\times H_s$=240 mm. A tensile loading σ=166.67 MPa is applied. The subscripts "*P*" stands for patch, "*S*" stands for sheet and "*A*" stands for adhesive. Table 1 gives the mechanical properties of the unidirectional carbon fiber reinforced plastic (CFRP) patch, the Aluminum alloy and the film adhesive.

2.2 Finite elements meshing

A 3D Finite elements Analysis is carried out using ABAQUS (2007) and considering only one-quarter of the repaired plate, due to symmetry. The finite element mesh was generated using the 20 nodes brick elements. Fig. 2 shows the meshing corresponding to one of the configurations used in the calculations.

In the present paper, the linear elastic fracture mechanics is applied for a homogenous plate where only mode 1 fracture is preponderant. Therefore, the Stress Intensity Factors SIF K_I is related to the energy release rate (*J* integral) through the following formula

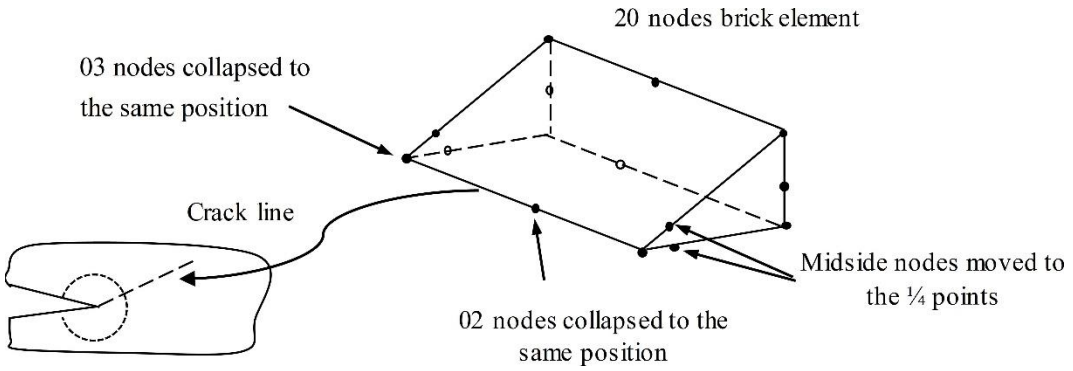

Fig. 3 Collapsed three dimensional element (20 nodes brick element)

$$J = \frac{K_I^2}{E(1-\upsilon^2)} \tag{1}$$

Where: E is the Young modulus, υ: the Poisson ratio.

The singularity at the crack tip should be considered to improve the accuracy of the J-integral and the stress intensity factors calculations. If r is the distance ahead of the crack tip, a $\sqrt{1/r}$ stress singularity must be created for elastic fracture applications. The 20-node bricks are used with a collapsed face where the nodes are constrained to move together. In addition to that, the midside nodes are moved to the 1/4 points, as illustrated in Fig. 3.

To refine the mesh near the crack tip, two requirements were set :

• The elements size is at least 1/120 of the half crack length within a circle of 0.8 mm diameter and the crack tip as a center

• The elements size is 1/40 of the half crack length within an area ranging from the previous circle to another circle of 4.8 mm diameter and the crack tip as a center.

In J-integral calculations, several contour integral evaluations are performed. Each contour can be considered as a ring of elements surrounding the nodes along the crack line from one crack face to the opposite crack face. However, J-integral estimates from different contours may vary. Mesh refinement is needed to find the contour integral value that is approximately constant. The requirements for mesh refinement near crack tip, mentioned above, were assumed after many trials until reaching this constant value of contour integral.

Depending on the varying dimensions of width and height during the parametric analysis, the total number of elements range from 45 000 to 50 000 elements.

2.3 Aim of the study

According to the description given in section 2.1, the crack length $2\times a$=24 mm is critical under the tensile loading σ=166.67 MPa. Such a plate has zero fatigue life. As explained by Kumar Mahadesh and Hakeem (2000), the repair can be applied such that the fatigue life of the repaired plate is restored to the same level as a plate without crack.

Therefore, the principal aim of this paper is to develop a metaheuristic method to optimize the patch shape, such that:

• The stress intensity factor SIF must be reduced to values lower than the fracture toughness

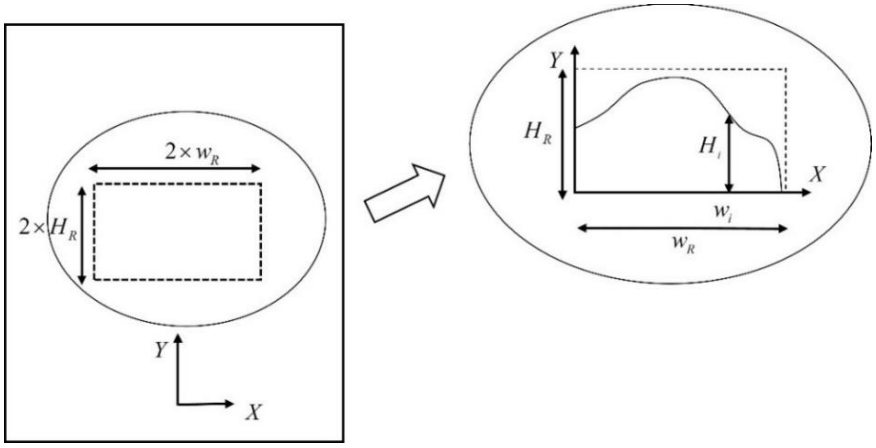

Fig. 4 Patch height as a function of its width

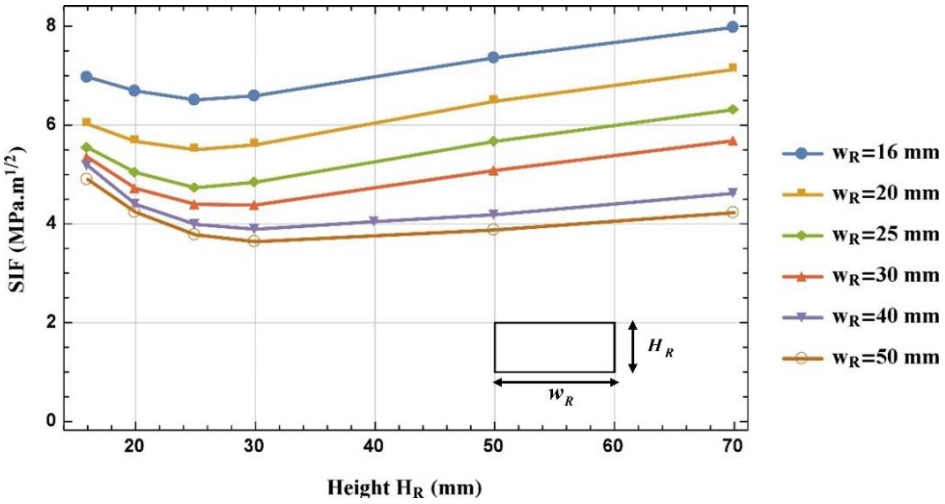

Fig. 5 Dimensions effect of a rectangular repair area

(improving fracture resistance)

• The stress intensity factor SIF must be reduced to the threshold SIF of the plate (restoring the fatigue life of the repaired plate to the same level as a plate without crack)

Taking the paper of Mahadesh Kumar and Hakeem as reference (2000), the fracture toughness $K_{IC} = 32.4MPa\sqrt{m}$ and the threshold SIF $K_{th} = 4.4MPa\sqrt{m}$.

Assuming the patch thickness t_p as constant, the optimization of the shape can be done by finding the best distribution of patch material over an area assumed fixed and equal to $4\times w_R\times H_R$=4×40×30 (mm^2). "*R*" stands for repair area over which the optimization will be carried out. One way to achieve this goal is to consider the patch height as a function of its width. For this purpose, the present optimization problem is directed towards finding this best function within a limited rectangular area, as shown in Fig. 4.

For a constrained optimization, the researcher can define the repair area $4\times w_R\times H_R$, as a matter of convenience. However, some considerations have been taken into account to define this area.

Fig. 5 illustrates the variation of SIF with respect to the dimensions of a rectangular repair area. The patch thickness is equal to 1.5 mm. The film adhesive thickness equals 0.15 mm. From Fig. 5, it is clear that there is a threshold value for H_R=30 mm beyond which the stress intensity factor SIF increases. A qualitative analysis of this figure shows also that the general rate of SIF variation changes slightly for width values w_R=40 mm and w_R=50 mm, with close values of SIF for the two widths.

Therefore and as a matter of convenience, the repair area of $4\times w_R\times H_R=4\times 40\times 30$ (mm^2) is assumed for the present constrained optimization problem.

Before developing this method, it will be helpful to look at the simple case, for which the height varies linearly with respect to patch width. The next section presents an introductory example to show the interaction between the repair height with its width. This aims at highlighting the need to find out the optimized distribution of height with respect to width, according to a well described mathematical method.

3. Skewed shapes as introductory examples

3.1 Geometry description

An introductory example is given to shed light on the issues to be addressed throughout this paper. From a rectangular patch, two shapes are constructed:

- A skewed shape with an increasing height (this is the Kumar and Hakeem model 2000). It will be called skewed shape type A.
- A skewed shape with a decreasing height. It will be called skewed shape type B.

Considering one-quarter of the repaired plate due to symmetry, Fig. 6 shows the dimensions associated with these shapes. The plate thickness is equal to 3 mm. The patch thickness is equal to 1.5 mm. The film adhesive thickness equals 0.15 mm. Now, the corresponding Stress Intensity Factors SIF are calculated to assess the effectiveness of these two shapes.

Maximal height is $H_{Max}=H_R$=30 mm, which is the height of the repair area assumed for the present constrained optimization (section 2.3). For convenience, ½ of the half-crack length is assumed for the minimal height $H_{Min}=\frac{a}{2}=6mm$. As explained in section 2.3, one value for acrack length is considered: it is the critical length under the tensile load σ=166.67 MPa.

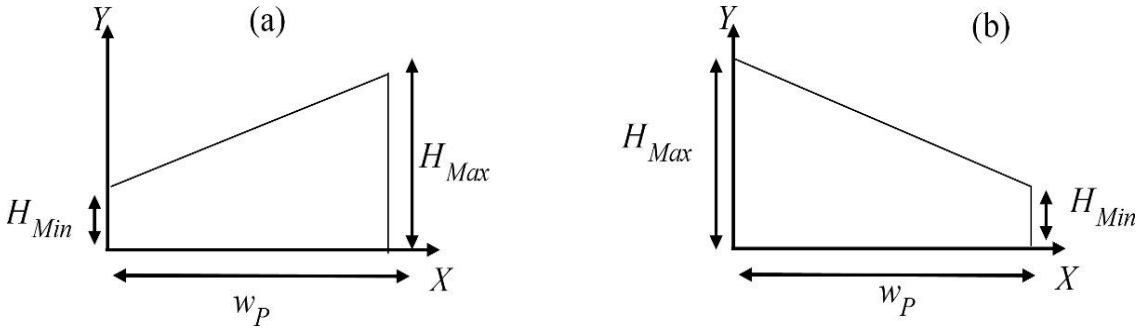

Fig. 6 Skewed shapes: (a) Skewed type A (b) Skewed type B

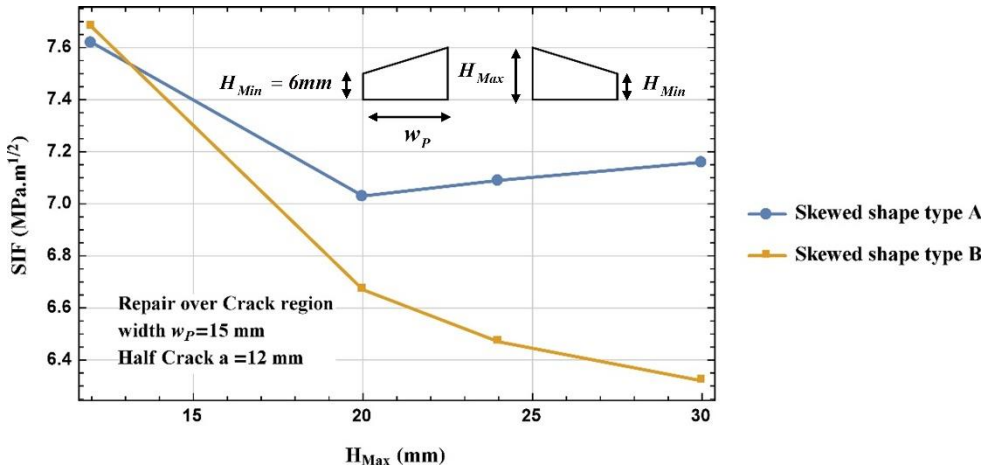

Fig. 7 SIF vs. H_{Max} for a repair performed over crack region (w_P=15 mm)

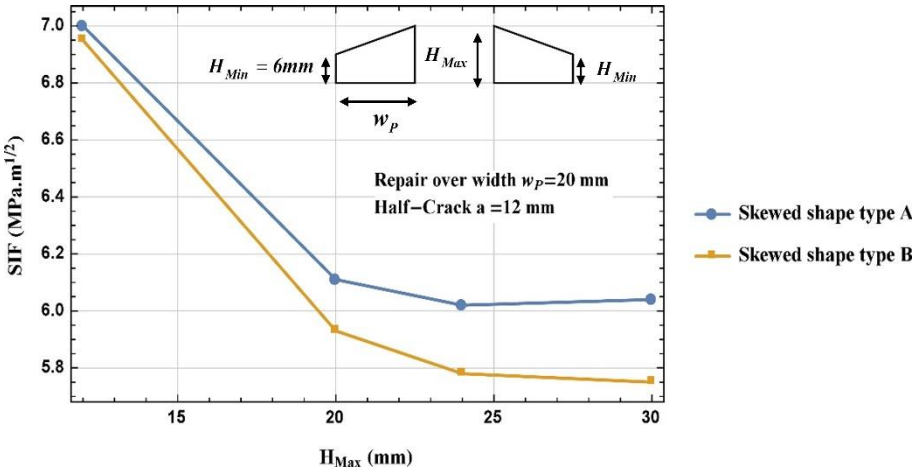

Fig. 8 SIF vs. H_{Max} for a repair performed over a width w_P=20 mm

3.2 Stress intensity factor variations

Fig. 7, Fig. 8, Fig. 9 and Fig 10 illustrate the differences between the repair efficiencies as the repair width varies when the two skewed shapes are applied. The following observations cases are identified:

- Repair over the crack region: where the width of the repair is not very long, compared with the crack length. In this case, the behavior of the two skewed shapes are different. While the SIF obtained with the skewed type B shows a continuously decreasing trend with respect to the ratio H_{Max}, the skewed type A presents a threshold value beyond which the SIF increases (Fig. 7).
- Repair over larger widths: this is the case where the repair width increases substantially compared to the crack length. More stressed regions are patched in the front of the crack tip. From Fig. 8, the two shapes show similar decreasing trend over larger range of height, up to H_{Max}=24 mm. Beyond this value, the shape type A shows an increasing trend. However, the

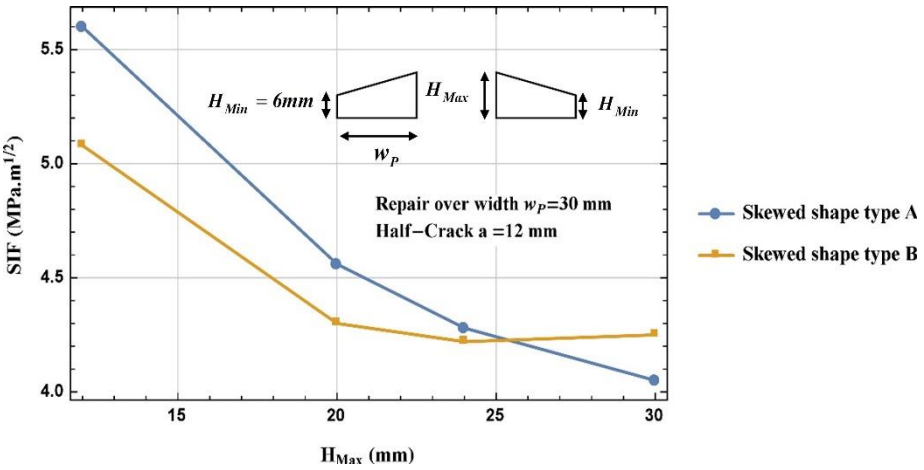

Fig. 9 SIF vs. H_{Max} for a repair performed over a width w_P=30 mm

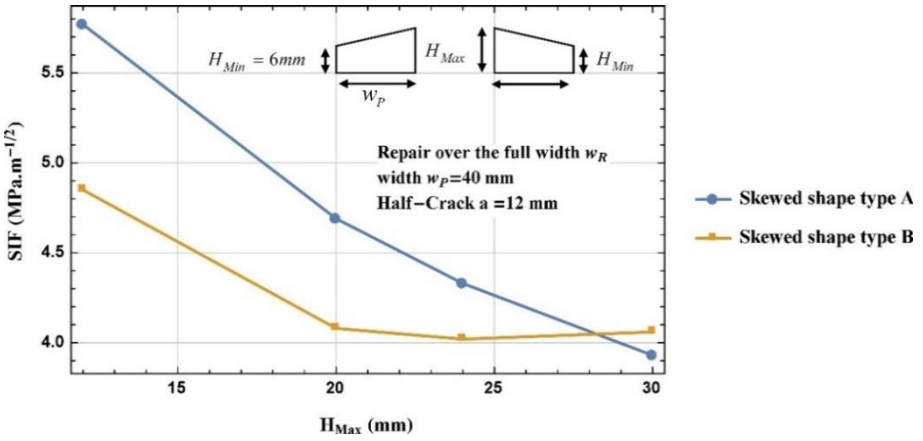

Fig. 10 SIF vs. H_{Max} for a repair performed over the total width w_P=40 mm

skewed shape type B remains still better than type A in reducing the SIF.

• As the patch width increases, lower values of SIF can be achieved with skewed type A if the ratio H_{Max} is sufficiently high (Figs. 9-10).

3.3 Adhesive shear stress variations

For repair effectiveness, it is desirable to keep the shear stresses in the adhesive as low as possible. Any repair design aims at allowing appropriate values for shear stresses to transfer loads from the plate to the patch, but without reaching very high values to avoid cohesive damage of the adhesive.

To analyze the shear stresses, the following ratio is calculated

$$R_{\tau} = \frac{\tau_{yz}}{\tau_{l}} \tag{2}$$

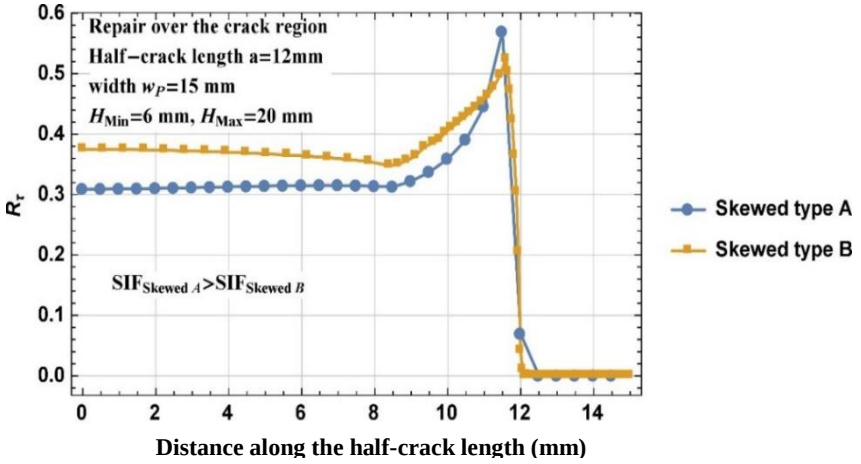

Fig. 11 Shear stress variation for a repair performed over crack region w_P=15 mm

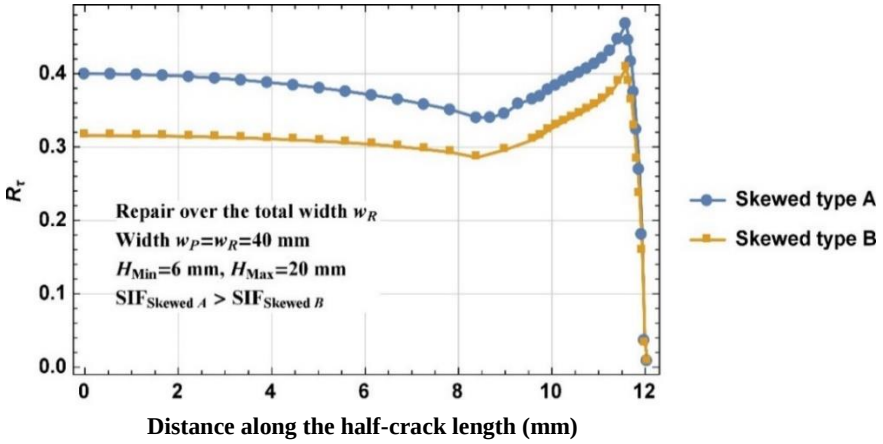

Fig. 12 Shear stress variation for a repair performed over the total width w_P=40 mm (Case H_{Max}=20 mm)

Where: τ_{yz} is the shear stress in the adhesive film along the half-crack side. τ_l is the linear limit shear stress.

As in the SIF analysis section (section 3.2), three cases can be identified:

• Repair over the crack region where the patch width is 1.25 times the crack length: Fig. 11 shows that the shear stress ratio R_τ is lower when the skewed type A is applied. While the skewed type B allowed reducing the SIF better than the skewed type A, it develops higher shear stresses. Therefore, an optimization is needed.

• Repair with patch width w_P=w_R=40 mm and H_{Max}=20 mm: This illustrates a case where the skewed type B is better than the skewed type A with respect to both SIF and shear stresses (Fig. 12)

• Repair over the width w_R=40 mm and H_{Max}=30 mm : Fig. 13 shows that both shapes produce similar values of shear stresses. Therefore, Skewed type A is better than type B since it allows obtaining the lower SIF value.

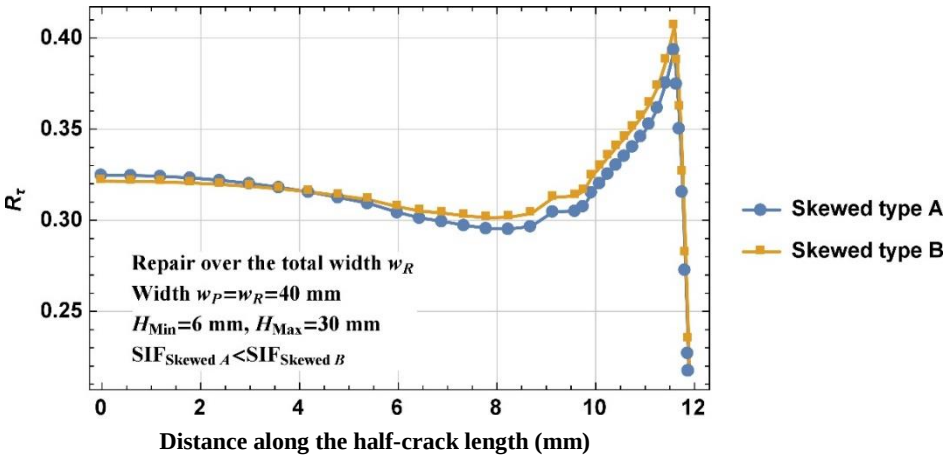

Fig. 13 Shear stress variation for a repair performed over the total width w_P=40 mm (Case H_{Max}=30 mm)

3.4 Concluding remarks

From the previous analysis, two regions are identified in the patch. The first region is lo-
cated behind the crack tip, where a decreasing repair height allowed better performance with respect to the SIF, but generated higher shear stresses in the adhesive. The second region lo-cated in front of the crack tip where the previous analysis have not brought out a clear conclusion about the best height trend.

There is a need to optimize both the SIF and the shear stresses taking into account the patch height distribution with respect to the repair width.

4. Optimization method

4.1 Bands-based model

The basic idea of the proposed model is to subdivide the patch area into five 05 bands. Two 02 bands within the crack region, and three 03 other bands in the remaining region of the patch outside the crack. One-quarter of the repaired plate is illustrated in Fig. 14. The choice of this subdivision is explained as follows:

- The first two bands, band 1 and band 2, have widths w_1=w_2=6 mm. They will model the patch height distribution over the half crack length (a=12 mm). Besides, the number of 02 bands was chosen to find out whether a, monotonically, increasing or decreasing height distribution over this region is preferred to get the best repair effectiveness.
- The three last bands, band 3, band 4 and band 5, will model the patch height distribution over the remaining repair region, in the front of the crack tip. The number of 03 bands is the lowest number, which can be assumed to investigate a non-monotonic variation of patch height over this region. Doing so, two-fold issues can be addressed. Firstly, the effect of patching will be analyzed in the highly stressed region ahead of the crack tip. Secondly, it will be possible to compare the obtained shape by the present method with other shapes found in literature, particularly the shape

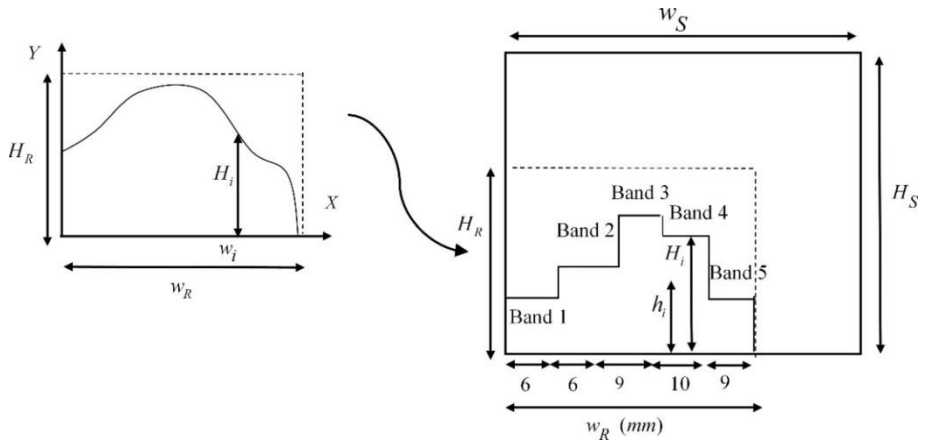

Fig. 14 Bands-based model as a patch height distribution

of Brighenti (2007) (with an increasing patch height in front of the crack tip) and the shape of Mhamdia Rachid *et al.* (2012) (with an arrow shape in front of the crack tip).

• The widths of the 03 last bands are chosen so that they have almost equal values to avoid any bias in the optimization calculations: $\frac{w_R - a}{3} = \frac{40-12}{3} = 9.33mm$. For convenience, integer values were preferred. So, the following values were chosen w_3=w_5=9 mm and the band in between has w_4=10 mm

The height of each band H_i can take one of the 04 discrete values, which are 6 mm, 12 mm, 24 mm or 30 mm. A point within a band is located at a distance h_i from the horizontal line. All the dimensions illustrated are in millimeter.

This model gives an approximation of the patch height distribution with respect to width. Hence, the optimal height distribution will be the optimal combination of bands heights.

4.2 Multi-objectives optimization and Pareto optimality concept

The aim of the present optimization task is to minimize three parameters (Objective functions):

• Stress Intensity Factor SIF
• Shear stress in the adhesive film
• Patch volume

$$\text{Problem objectives} \begin{cases} Minimize(SIF) \\ Minimize(R_{\tau\ peaks}) \\ Minimize(patch\ Volume) \end{cases} \tag{3}$$

For each $i \in \{1,2,3,4,5\}$, H_i can take the values

$$\begin{cases} x_{ij} = 6\ mm\ if\ \ j = 1 \\ x_{ij} = 12\ mm\ if\ j = 2 \\ x_{ij} = 24\ mm\ if\ j = 3 \\ x_{ij} = 30\ mm\ if\ j = 4 \end{cases} \tag{4}$$

Therefore, there are 05 variables H_i. Each of them can take 04 discrete values x_{ij}.

Besides, the shear stresses will be expressed as follows

$$R_{\tau\ peaks} = Mean\left(\frac{\tau_{yz\ \text{peaks}}}{\tau_l}\right) \tag{5}$$

This is the mean value of the shear stress peaks recorded on the half-crack side, where high shear strain is developed, as mentioned by Papanikos *et al*. (2007). The high shear stress at free edges will be addressed in a separate future study.

The problem, as formulated, consists of finding a set P^* of the best combinations $\left(H_1^*, H_2^*, H_3^*, H_4^* H_5^*\right)$. Mathematically speaking, a combination $\left(H_1^*, H_2^*, H_3^*, H_4^* H_5^*\right)$ is a non-dominated solution according to the Pareto optimality concept. Among a set P of candidate solutions S, a non-dominated solution S^* must satisfy the following conditions:

- The solution S^* is no worse with respect to all objectives
- The solution S^* is, at least, better than the other solutions with respect to one objective
- In addition to that, any solution not belonging to P^*must be dominated at least by one member of P^*

To explain further this concept, let's take the case of 02 objectives to be minimized, Obj_1 and Obj_2 (as in the case of minimizing SIF and patch volume). Generally, SIF and patch volume are conflicting objectives. An incremental increase in patch volume produces a corresponding decrease in SIF, and vice versa. The typical variation of such 02 objectives can be illustrated in Fig. 15

The solutions S^D are dominated by the solutions S^* belonging to the Pareto curve. For instance, the solutions S_1^* and S_2^*, on Fig. 15, dominate the solution S^D because they satisfy

$$\begin{cases} Obj_1\left(S_1^*\right) < Obj_1\left(S^D\right) \\ Obj_2\left(S_1^*\right) < Obj_2\left(S^D\right) \\ Obj_1\left(S_2^*\right) < Obj_1\left(S^D\right) \\ Obj_2\left(S_2^*\right) < Obj_2\left(S^D\right) \end{cases} \tag{6}$$

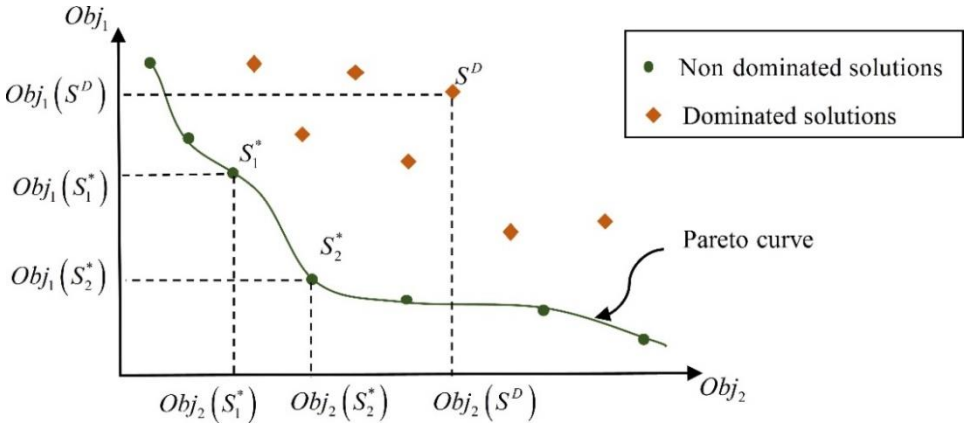

Fig. 15 Illustration of Pareto curve in the case of 02 objectives problem

Besides, the 02 solutions S_1^* and S_2^* are non-dominated solutions and they satisfy

$$\begin{cases} Obj_1\left(S_1^*\right) > Obj_1\left(S_2^*\right) \\ Obj_2\left(S_1^*\right) < Obj_2\left(S_2^*\right) \end{cases} \tag{7}$$

The best solutions belong the Pareto curve. In the case of 03 objectives, the best solutions belong to a Pareto surface. A non-dominated solution S^* represents the heights of the 05 bands $\left(H_1^*, H_2^*, H_3^*, H_4^* H_5^*\right)$. Therefore, the Pareto surface gives the set of the best shapes.

The non-dominated solutions will be found using the Naïve and Slow algorithm (Deb 2001).

4.3 Estimation distribution algorithm

Estimation distribution approach stands for a class of metaheuristic methods (Hauschild and Pelikan 2011). The principal idea consists of an initial random sampling of candidate solutions from a joint probability distribution. Then, an iterative process is undertaken to select and generate new interesting solutions through a Bayesian learning method. Without entailing the mathematical derivations (Neapolitan 2004, Hauschild and Pelikan 2011), the present methods consist of the following steps:

4.3.1 Bands-based model as a Bayesian network

The patch height distribution illustrated in Fig. 14 will be represented as a Bayesian network (Fig. 16). The height of each band H_i is considered as a random variable. The value x_{ij} taken by the variable H_i will be conditionally dependent on the value x_{i-1k} taken by the variable H_{i-1}. This is expressed by the conditional probability

$$\Pr(H_i = x_{ij} / H_{i-1} = x_{i-1k}) = \frac{\alpha_{ijk}}{\alpha_{ijk} + \beta_{ijk} + \gamma_{ijk} + \eta_{ijk}} \tag{8}$$

Where: $i \in \{1,2,3,4,5\}$, $j \in \{1,2,3,4\}$, $k \in \{1,2,3,4\}$. The coefficients α_{ijk}, β_{ijk}, γ_{ijk} and η_{ijk} are the Parameters of the corresponding Dirichelt probability Distribution (Neapolitan 2004).

For instance, if $\alpha_{21k}=\beta_{21k}=\gamma_{21k}=\eta_{21k}=1$, then the variable H_2 can take one of the 04 possible values $x_{2j}(j \in \{1,2,3,4\})$ depending on the value $x_{1k}(j \in \{1,2,3,4\})$ taken by H_1 according to a uniform probability distribution

$$\begin{cases} \Pr(H_2 = x_{21} / H_1 = x_{1k}) = \dfrac{1}{4} \\ \Pr(H_2 = x_{22} / H_1 = x_{1k}) = \dfrac{1}{4} \\ \Pr(H_2 = x_{23} / H_1 = x_{1k}) = \dfrac{1}{4} \\ \Pr(H_2 = x_{24} / H_1 = x_{1k}) = \dfrac{1}{4} \end{cases} \quad k \in \{1,2,3,4\} \tag{9}$$

4.3.2 Generating and selecting shapes

Initially, each band has a uniform probability distribution to take one of the 04 values x_{ij}, according to Eqs. (8)-(9). From this distribution, an initial random population is sampled

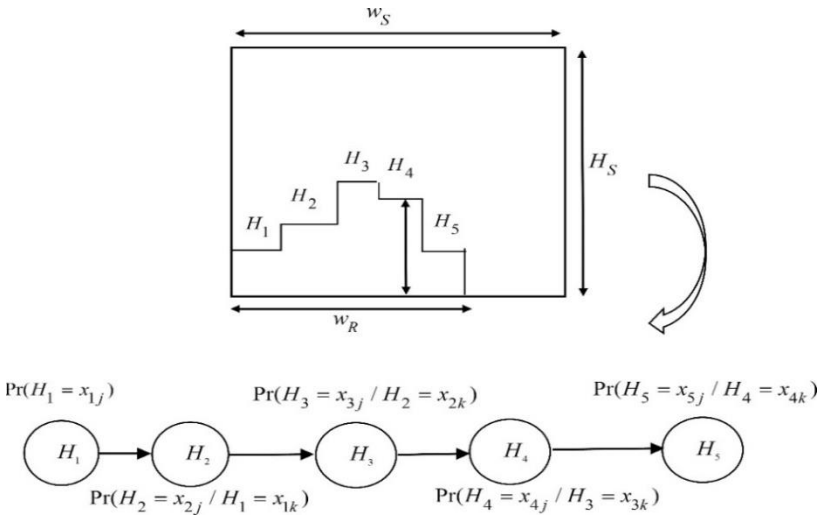

Fig. 16 Bayesian network representation of the Bands-based model

$$P_1 = \{(H_1, H_2, H_3, H_4, H_5)_{(1)}, ..., (H_1, H_2, H_3, H_4, H_5)_{(N)}\} \tag{10}$$

This is a set of N patch shapes at iteration 1. Then, the set P_1^* of non-dominated solutions is determined using the Naïve and slow algorithm (Deb 2001). Then, the coefficients α_{ijk}, β_{ijk}, γ_{ijk} and η_{ijk} are updated to give the conditional probability distributions that would produce the set P_1^*. The mathematical details of this updating procedure are demonstrated in references on Bayesian reasoning such as (Neapolitan 2004).

The next population P_2 (population at iteration 2) is constructed so that each member belonging to P_2, is not dominated by a member of P_1. It will be given by

$$P_2 = P_1 \cup P_1^{(updt)} \tag{11}$$

Where: $P_1^{(updt)}$ is a population constructed using the coefficients α_{ijk}, β_{ijk}, γ_{ijk} and η_{ijk} updated at iteration1.

The same procedure is repeated for the next iterations.

4.3.3 Running the iterative process

As any convergent iterative process, calculations can be stopped when:

- A number of iteration is reached
- A threshold value is reached

For the sake of simplicity, a minimum number of iterations will be used to make qualitative interpretations. The present iterative process must be kept running until finding shapes reducing both SIF and patch volume better than the skewed shapes of Fig. 3. Kumar Mahadesh and Hakeem (2000) were the first researchers who analyzed the skewed shape type A, and he found that it is very effective in crack repair when it satisfies the following formula

$$0.6 \leq \frac{H_{Max} - H_{Min}}{w_P} \prec 0.7 \tag{12}$$

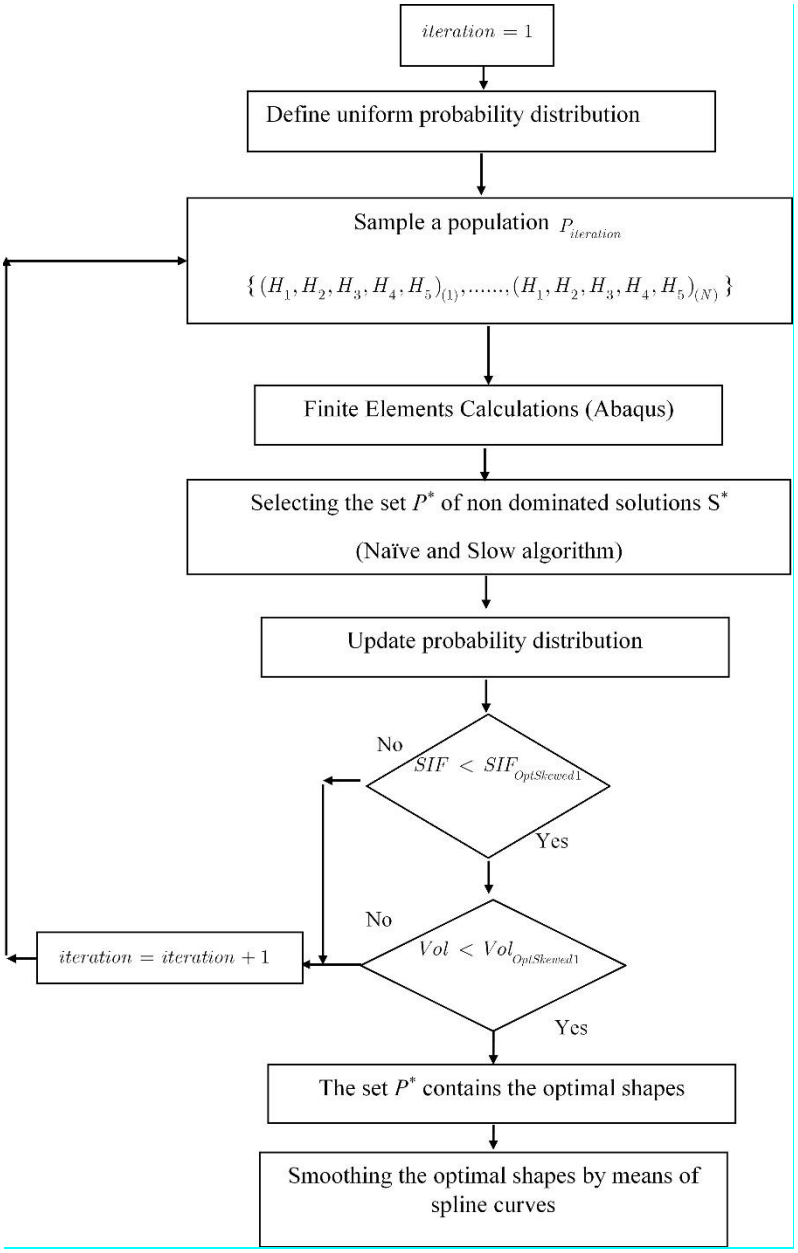

Fig. 17 Optimization algorithm

Brighenti *et al*. (2006, 2007) confirmed his finding. Therefore, the smallest number of iterations must be sufficient to meet two conditions:

• The SIF is lower than a threshold value. To this end, the threshold value is taken as the SIF obtained by applying the optimized skewed shape type A

• The patch volume *Vol* is lower than the optimized volume of the optimized skewed shape type A ($Vol_{OptSkewed1}$).

As our optimization is performed over an area $w_R \times H_R$=40 mm×30 mm, the skewed shape chosen for comparison must satisfy $\frac{H_{\max} - H_{Min}}{w_P} = 0.6$, which corresponds to H_{Min}=6 mm, H_{Max}=30 mm, w_P=40 mm. Fig. 17 summarizes the steps of the algorithm.

5. Implementation and results

5.1 Data and running the algorithm

For numerical implementation, the materials described in section 2 are taken with the following thicknesses:

- Plate thickness equal to 2 mm
- Composite patch thickness equal to 1 mm
- Adhesive film thickness equal to 0.125 mm

The mechanical properties are mentioned in Table 1. According to the explanation given in section 4.3.3, the threshold values are $SIF_{OptSkewed1}$=2.77 MPa.m$^{1/2}$, and $Vol_{OptSkewed1}$=720 mm^3.

As explained in the previous section, the present optimization method aims at finding a set of several shapes, which satisfy the Pareto optimality concept. At each iteration, the algorithm identifies the best shapes set $P^*_{Iteration}$ from the sampled candidate shapes $P_{Iteration}$. Among the shapes S^* of the set $P^*_{Iteration}$, the lowest SIF values are plotted against the iteration (Fig. 18). From the second iteration, the algorithm identified shapes reducing the SIF more than the skewed shape. Nevertheless, the iterative process continues to find out shapes reducing both SIF and patch volume, while keeping the shear stresses as low as possible.

5.2 Analysis of optimal shapes

Tables 2-3 give the geometric dimensions of optimum shapes, after 07 iterations. These are the

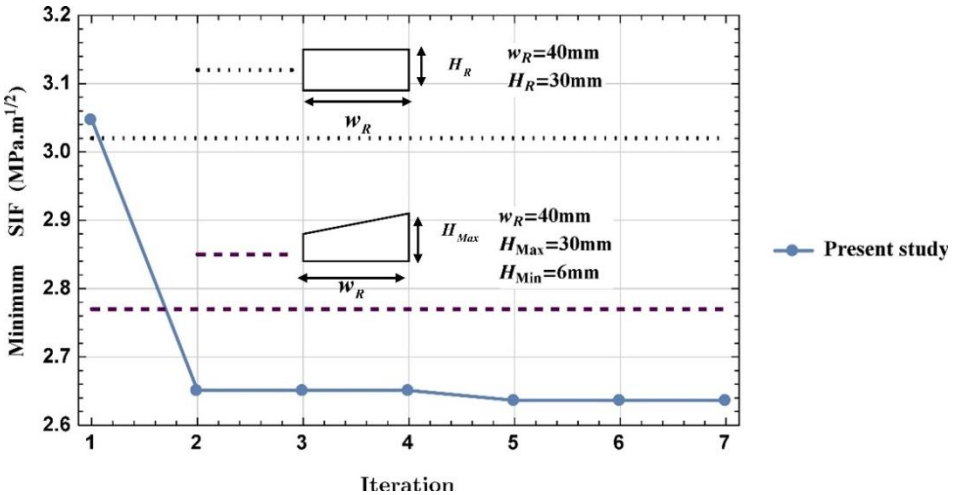

Fig. 18 SIF reduction through 7 iterations

Table 2 Optimal shapes (category 1)

Shapes $\left(H_1^*, H_2^*, H_3^*, H_4^* H_5^*\right)$		SIF(MPa.m$^{1/2}$)	Patch volume (mm^3)	$R_{\tau\,\text{peaks}}$
Shape Opt1	(24,6,24,30,30)	2.63	966	0.26
Shape Opt2	(30,12,6,30,30)	2.65	876	0.28
Shape Opt3	(24,6,12,24,12)	2.68	636	0.29
Shape Opt4	(24,6,12,24,6)	2.73	582	0.295
Comparison				
Rectangle: w_P=W_R=40 mm, H_P=H_R=30 mm		3.8	1200	0.28

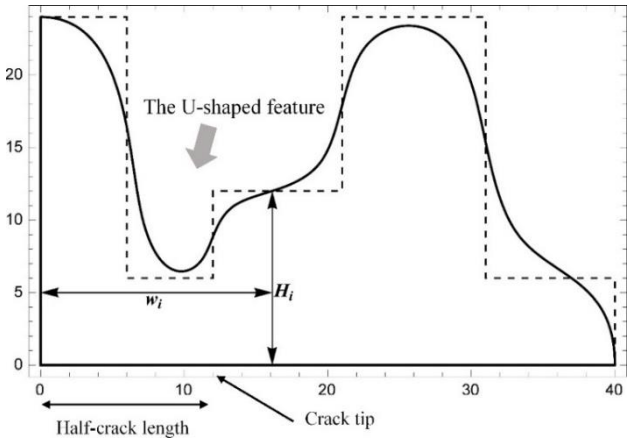

Fig. 19 The U-shaped feature (example of shape Opt4)

dimensions of one-quarter of the repaired plate. For the sake of clarity, the solutions are presented in two categories:

- Category 1: it contains the shapes for which, the $SIF \prec 3MPa.m^{1/2}$
- Category 2: it contains the shapes for which, the $3MPa.m^{1/2} \le SIF \le 3.8MPa.m^{1/2}$

This distinction is a matter of convenience and it makes the results interpretation easier and clearer.

For the 02 categories, the SIF values are lower than the threshold $SIF\ \ K_{th} = 4.4MPa\sqrt{m}$. Therefore, the fatigue life of the repaired plate is restored to the level of a plate without crack, as explained in section 2.3.

Looking at these dimensions, an outstanding geometric feature can be noticed. There is a "U-shaped feature" formed around the crack tip.

This feature characterizes all the shapes (category 1) found by the algorithm. For instance, Fig. 19 exhibits the "U-shaped feature" for the shape Opt4$\left(24,6,12,24,6\right)$, by means of spline curves (de Boor 2001).

Spline curves will be used for all the optimal shapes obtained by the algorithm. The curves are constructed using basis spline function associated with control points (de Boor 2001). These points are the vertices of the 05 bands used in the model. For the shape Opt4, the control points and their Cartesian coordinates are shown on Fig. 20.

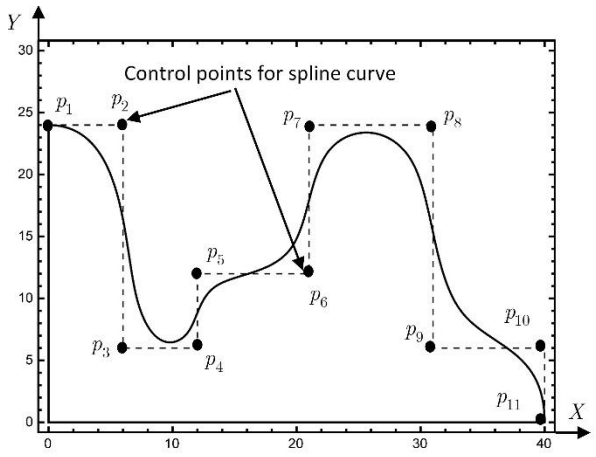

	X (*mm*)	Y (*mm*)
Point p_1	0	24
Point p_2	6	24
Point p_3	6	6
Point p_4	12	6
Point p_5	12	12
Point p_6	21	12
Point p_7	21	24
Point p_8	31	24
Point p_9	31	6
Point p_{10}	40	6
Point p_{11}	40	0

Fig. 20 Control points for spline curve (example of shape Opt4)

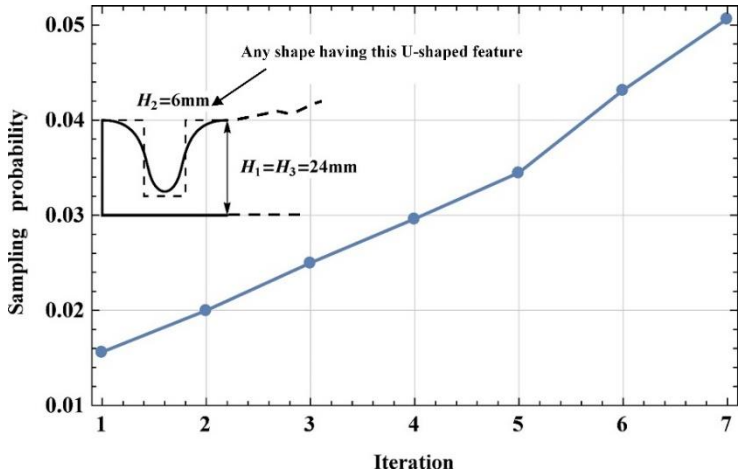

Fig. 21 The likelihood of the U-shaped feature during the searching of shapes

By means of computer programming, the basis spline function associated with the control points, is used to plot the patch profile as in Fig. 20. The same technique will be used for the other shapes.

As a probabilistic demonstration, Fig. 21 shows an increase in the likelihood of the development of this U-shaped feature through iterations. As the searching process of candidate shapes progresses, it becomes more likely to sample shapes having this U-shaped feature over the crack region, whatever the values of H_4 and H_5.

Shapes Opt1-Opt2 are the lowest SIF shapes identified by the algorithm. Fig. 22 illustrates how the patch material distribution improves the repair through SIF reduction. The first band represents the patch region where stiffness increase contributes to prevent the crack faces from opening. In the front of the crack tip, the region is characterized by a transition zone where the patched area is increasing progressively. The fourth band allows patching higher stresses regions in the cracked plate.

The performances of the two shapes in reducing adhesive shear stresses are different (see Table 2

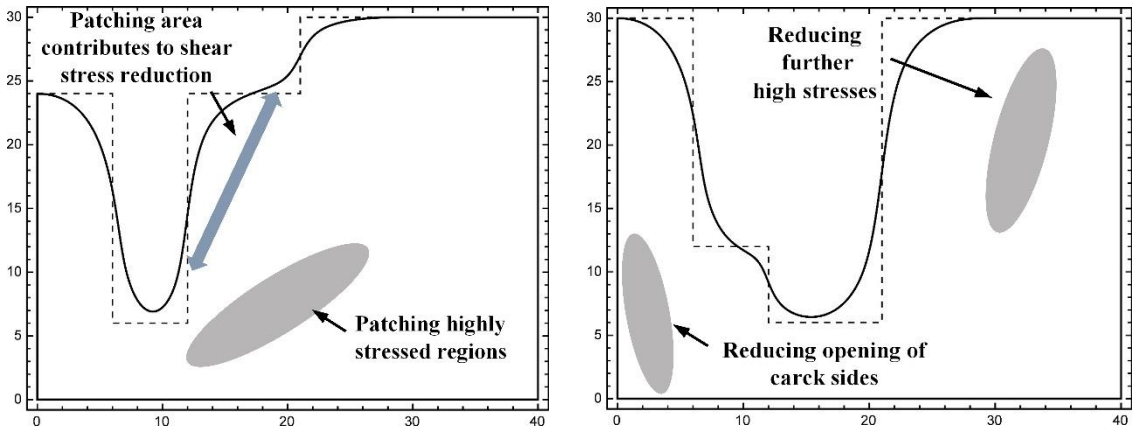

(a) Optimal Shape Opt1 (b) Optimal Shape Opt2

Fig. 22 illustration of patch material distribution effect for shapes Opt1-Opt2

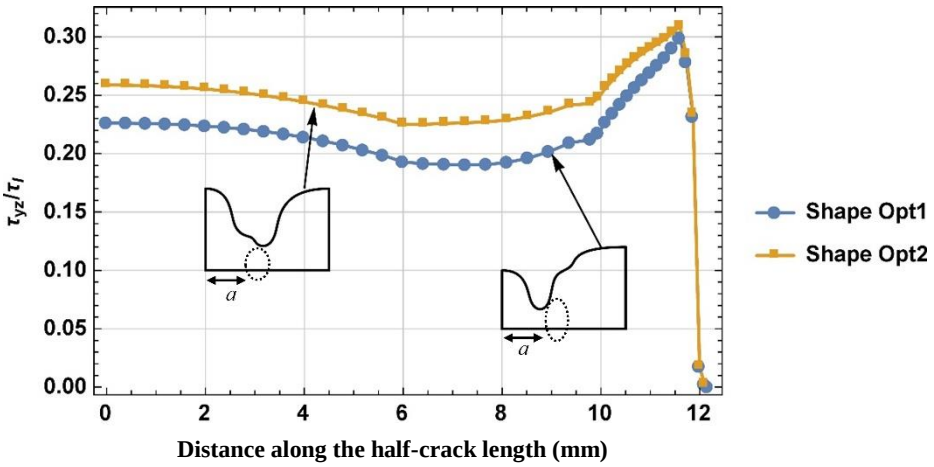

Fig. 23 adhesive shear stresses for optimal shapes Opt-1 and Opt-2

and Fig. 23). Shape Opt1 develops lower shear stresses in the adhesive film, because of its extended patched area near the crack tip front (as illustrated in Fig. 22(a) and 23).

Far from the crack tip, the fifth band has an impact on reducing the SIF, but the algorithm shows that the patched area over this far region can be reduced to gain mass. This is explained through analyzing shapes Opt3 and Opt4. Fig. 24 compares between the patch material distributions for these two shapes:

This can be highlighted further by defining the marginal mass gain and the marginal SIF reduction

$$\partial Gain_{Mass}(Shape\ Opt4) = \frac{Volume(Opt3) - Volume(Opt4)}{Volume(Opt3)} \times \frac{SIF(Opt4)}{SIF(Opt4) - SIF(Opt3)}(\%) \quad (13)$$

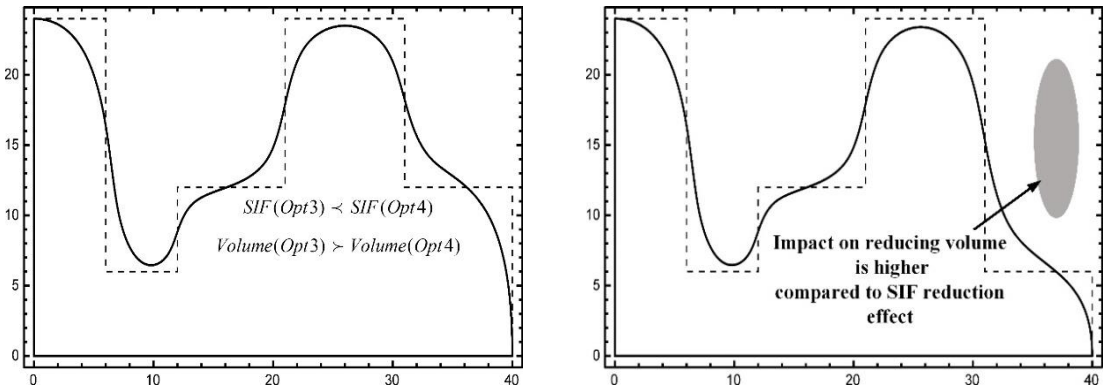

(a) Optimal Shape Opt3 (b) Optimal Shape Opt4

Fig. 24 patch material distribution for shapes Opt3 and Opt4

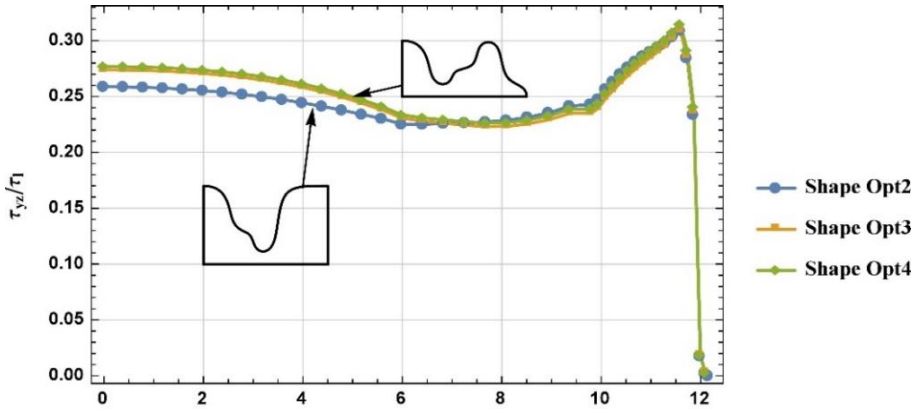

Fig. 25 adhesive shear stresses for optimal shapes Opt-3 and Opt-4 (compared to Opt2)

$$\partial \,\mathrm{Re}\,duction_{SIF}\,(Shape\ Opt3) = \frac{SIF(Opt4) - SIF(Opt3)}{SIF(Opt4)} \times \frac{Volume(Opt3)}{Volume(Opt3) - Volume(Opt4)}(\%) \qquad (14)$$

Eqs. (13)-(14) are applied to shapes Opt3-Opt4, since they are similar except in the height of the fifth band H_5. It is found that 4.67% of mass can be gained by allowing 1% increase in the SIF. However, only 0.19% in SIF reduction is obtained through 1% of increase in patch volume. This result shows that the effect of the fifth band (region far from the crack tip, in Fig. 24(b)) is more related to mass gain than SIF reduction.

As far as the adhesive shear stresses are concerned, the two shapes Opt3 and Opt4 are closely similar (Fig. 25). The increase in patched area over the fifth band region (far from the crack tip) has no great effect on adhesive shear stresses.

Shape Opt1 is the best shape for reducing shear stresses. It has a greater patched area in the front of the crack tip. Shapes Opt3-Opt4 generate shear stresses higher than those generated by the other optimal shapes of category 1. However, they have lower volumes. Therefore, the algorithm gives

families of optimal shapes. The choice of one of these shapes will depend on design considerations. This issue will be addressed in the section 5.3.

Table 3 gives optimal shapes of category 2, for which 3 MPa.m$^{1/2}$≤*SIF*≤3.8 MPa.m$^{1/2}$:

These shapes have the lowest volumes and they are better than rectangular shape for reducing SIF. They allow up to 65% gain in patch volume (patch mass). However, they develop higher shear stresses. Fig. 26 shows the shear stresses developed by these shapes, Opt5 and Opt6:

These high stresses are caused by the reduced patched area within the third band (near the crack tip front). Shape Opt6 is a special case where the U-shaped feature around the crack tip is not developed. These shapes allow reducing a great amount of patch volume. The algorithm identified them as optimal according to Pareto optimality concept.

Fig. 27 illustrate the patch material distribution for these two shapes:

5.3 Comparison and selection among the optimal shapes

This section will define a criterion to compare between the optimal shapes identified in the previous section. For this purpose, weight functions are defined

$$Weight_{SIF}(Shape\ Opt"i") = F_{SIF}/F_{Total} \tag{15}$$

$$Weight_{Volume}(Shape\ Opt"i") = F_{Volume}/F_{Total} \tag{16}$$

Table 3 Optimal shapes (category 2)

Shapes $(H_1^*, H_2^*, H_3^*, H_4^* H_5^*)$		SIF(MPa.m$^{-1/2}$)	Patch volume (mm^3)	$R_{\tau\ \text{peaks}}$
Shape Opt5	(24,6,12,12,6)	3.07	462	0.32
Shape Opt6	(60,12,6,6,6)	3.55	420	0.36
Comparison				
Rectangle w_P=W_R=40 mm, H_P=H_R=30 mm		3.8	1200	0.28

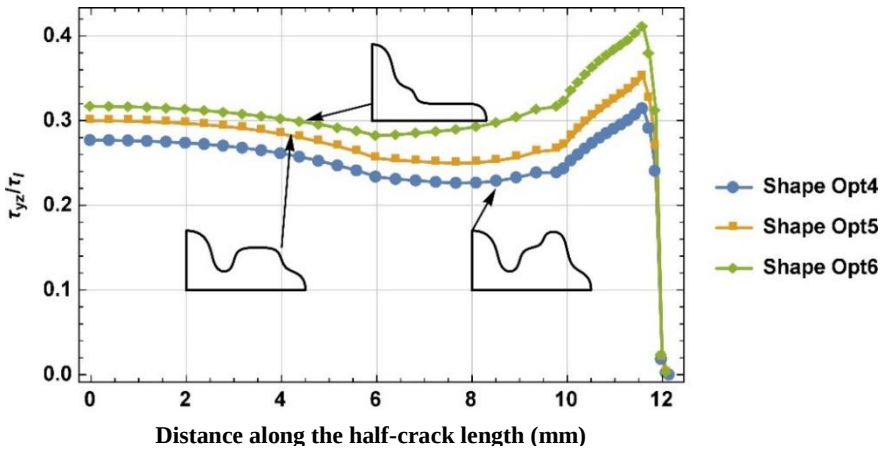

Fig. 26 Adhesive shear stresses for shapes Opt5 and Opt6 (compared to Opt4)

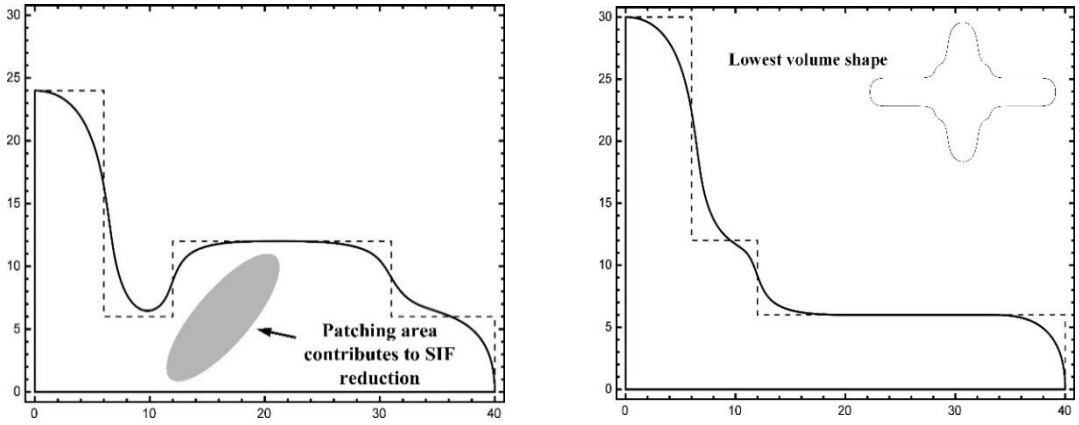

(a) Optimal Shape Opt5 (b) Optimal Shape Opt6

Fig. 27 Patch material distribution of the lowest volumes shapes: Opt5 and Opt6

$$Weight_{Shear}(Shape\ Opt"i") = F_{Shear}/F_{Total} \tag{17}$$

$$F_{SIF} = \left(\frac{SIF^{Max} - SIF\left(Opt"i"\right)}{SIF^{Max} - SIF^{Min}} \right) \tag{18}$$

$$F_{Volume} = \left(\frac{Volume^{Max} - Volume\left(Opt"i"\right)}{Volume^{Max} - Volume^{Min}} \right) \tag{19}$$

$$F_{Shear} = \left(\frac{R^{Max}_{\tau\ peaks} - R_{\tau\ peaks}\left(Opt"i"\right)}{R^{Max}_{\tau\ peaks} - R^{Min}_{\tau\ peaks}} \right) \tag{20}$$

$$F_{Total} = F_{SIF} + F_{Volume} + F_{Shear} \tag{21}$$

From the obtained set of optimal solutions:

- SIF^{Max} and SIF^{Min} are the maximum and minimum values of *SIF*
- $Volume^{Max}$ and $Volume^{Min}$ are the maximum and minimum values of patch volume
- $R^{Max}_{\tau\ peaks}$ and $R^{Min}_{\tau\ peaks}$ are the maximum and minimum values of shear stress ratio

"Rectg" is the rectangular shape: w_P=w_R=40 mm, H_P=H_R=30 mm.

From Tables 2-3, these values are

$$\begin{cases} SIF^{Max} = SIF\ \ (\mathrm{Re}ctg) \\ SIF^{Min} = SIF\ \ (Opt1) \\ Volume^{Max} = Volume\ \ (\mathrm{Re}ctg) \\ Volume^{Min} = Volume\ \ (Opt6) \\ R^{Max}_{\tau\ peaks} = R_{\tau\ peaks}\ (Opt6) \\ R^{Min}_{\tau\ peaks} = R_{\tau\ peaks}\ (Opt1) \end{cases} \tag{22}$$

Table 4 weighting functions of optimal shapes, skewed and rectangular shapes

Shapes	$Weight_{SIF}$ (%)	$Weight_{Volume}$ (%)	$Weight_{Shear\ stress}$ (%)	Standard deviation of the 03 weights
Shape Opt1	43.8	13.15	42.99	17.47%
Shape Opt2	45.03	19.03	35.93	13.19%
Shape Opt3	40.44	30.55	28.99	6.2%
Shape Opt4	39.01	33.8	27.18	5.9%
Shape Opt5	31.79	48.21	19.98	14.17%
Shape Opt6	17.6	82.39	0	43.39%
Optimized skewed shape type A	35.27	24.65	40.07	7.88%
Rectangular shape w_P=w_R=40 mm, H_P=H_R=30 mm	0	0	1	57.73%

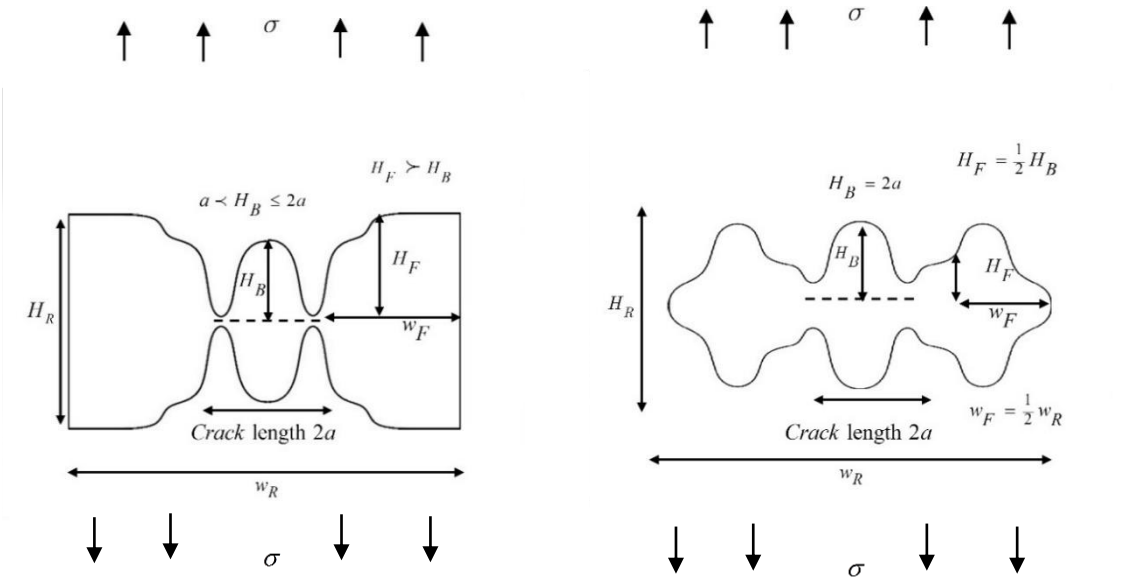

(a) patch shape giving high weights for SIF and adhesive shear stresses reductions

(b) patch shape giving equal weights for SIF , volume and adhesive shear reductions

Fig. 28 Optimal shapes

Eqs. (15)-(17) calculate the relative distance of a solution from the worst (maximum) value in each objective (Deb 2001). For each objective, the maximum value of the weight function corresponds to the best solution for this objective. The worst value for an objective is the maximum value because it is a minimization problem. Results are presented in Table 4.

The designer would choose the shape that is closer to the preferred weight function. For instance, if designer's preference is focused on reducing SIF and adhesive shear stresses, shape Opt1 would be the best. Compared to rectangular shape, it gives an additional 30.78% reduction in SIF and an additional 19.5% gain in patch volume. Fig. 28(a) illustrates the geometric feature of this shape.

However, all the objectives are important. Designer's preference might be oriented towards reducing equally the three objectives. The statistical parameter, called Standard Deviation, measures the dispersion in the values of the three weights. It provides a tool to assess how the weights are distributed around a mean value. The smaller the standard deviation, the more narrow the range between the lowest and highest weights for a given shape. In other words, the weights cluster closely to the mean value. In this case, SIF, patch volume and adhesive shear stress will have closely similar weights. From table 4, it is clear that shape Opt4 has the lowest standard deviation, around 6%.

Compared to rectangular shape, it gives an additional 28.15% in SIF and a considerable 51.5% gain in patch volume. Fig. 28(b) shows this shape.

This study shed more light on shape optimization for fracture repair. Unlike other optimization models, it is a multi-objective method, which provides families of shapes. One of the shapes identified by the present algorithm (Fig. 28(a)) is similar to a shape found by Brighenti (2007) using genetic algorithm. However, the present method has shown, by means of explicit probability formulation that this shape is the best only if designer's preference or repair requirements are focused exclusively on SIF and shear stress reductions. Otherwise, another shape has been identified which is better with respect to SIF, shear stresses and patch volume reductions (Fig. 28(b) and Table 4).

Table 5 provide a qualitative comparison between the present method and some references.

Table 5 Summary of some references addressing the patch shape optimization

	Optimization method Principal results	Comments
Kumar Mahadesh and Hakeem 2000	• Parametric analysis was carried out • No mathematical method was developed for optimization purposes • A skewed shape was obtained • The skewed shape was found more effective than rectangular patch in reducing SIF (the two shapes with similar volumes)	The SIF was the objective to be minimized
Brighenti 2007	• Genetic algorithm for optimization purposes • Optimum shape obtained through an iterative process	• The first study (as the knowledge of the authors) developing a mathematical method to optimize patch shape. • One objective to be minimized (SIF)
Mhamdia Rachid *et al*. 2012	• Parametric analysis was carried out • No mathematical method was developed for optimization purposes • An "arrow shape" was obtained	SIF was the objective to be minimized.
Kashfuddoja and Ramji 2014	• Octagonal shape was chosen as a result of a parametric study • Genetic algorithm was used to obtain optimum dimensions for that shape	Stress Concentration Factor was the objective to minimize.
Present paper	• Probabilistic approach and Estimation Distribution algorithm were used • Optimum shape is obtained through an iterative process • Families of shapes were obtained	• Three objectives to minimize: SIF, patch volume and adhesive shear stress • A method to include designer's preferences in the comparison between the optimal shapes.

6. Conclusions

A probabilistic optimization method has been developed to find out the best patch shape for improving cracked plate repair. It aimed to minimize three objectives: stress intensity factor as fracture resistance criterion, patch volume to gain mass and adhesive shear stresses to enhance the adhesion durability between the fractured plate and the composite patch. The implementation of the method has brought out families of optimal shapes with specific geometric features around the crack tip and the horizontal end of the patch. Criteria were defined to choose one of theses shapes depending on technical repair requirements. This method has shown considerable mass gain while improving the repair effectiveness and keeping the adhesive shear stress at low levels.

References

ABAQUS (2007), ABAQUS Standard/User's Manual, Version 6.5, Hibbit Karlsson & Sorensen, Inc, Pawtucket, RI, USA.

Achour, T., Bachir Bouiadjra, B. and Serier, B. (2003), "Numerical analysis of the performances of the bonded composite patch for reducing stress concentration and repairing cracks at notch", *Comput. Mater. Sci.*, **28**, 41-48.

Baker, A., Rose, L.R.F. and Jones, R. (2002), *Advances in the Bonded Composite Repair of Metallic Aircraft* Structure, Volume 1, Elsevier, Kidlington, Oxford, UK.

Belhouari, M., Bachir Bouidjra, B., Megueni, A. and Kaddouri, K. (2004), "Comparison of double and single bonded repairs to symmetric composite structures: a numerical analysis", *Compos. Struct*., **65**, 47-53.

Brighenti, R., Carpinteri, A. and Vantadori, S. (2006), "A genetic algorithm applied to optimisation of patch repairs for cracked plates", *Comput. Meth. Appl. Mech. Eng*., **196**, 466-475.

Brighenti, R. (2007), "Patch repair design optimisation for fracture and fatigue improvements of cracked plates", *Int. J. Solid. Struct.*, **44**, 1115-1131.

Deb, K. (2001), *Multi-objective Optimization using Evolutionary Algorithms*, John Wiley & Sons Ltd, England, UK.

De Boor, C. (2001), *Practical Guide to Splines*, Springer-Verlag, New York, Inc.

Gu, L., Ram, A., Kasavajhala, M. and Zhao, S. (2011), "Finite element analysis of cracks in aging aircraft structures with bonded composite-patch repairs", *Compos. Part B*, **42**, 505-510.

Hauschild, M. and Pelikan, M. (2001), "An introduction and survey of estimation of distribution algorithms", *Swarm Evol. Comput.*, **1**, 111-128.

Jamal-Omidi, M., Falah, M. and Taherifar, D. (2014), "3-D fracture analysis of cracked aluminum plates repaired with single and double composite patches using XFEM", *Struct. Eng. Mech.*, **50**(4), 525-539.

Kaddouri, K., Ouinas, D. and Bachir Bouiadjra, B. (2008), "FE analysis of the behaviour of octagonal bonded composite repair in aircraft structures", *Comput. Mater. Sci.*, **43**, 1109-1111.

Kashfuddoja, M. and Ramji, M. (2014), "Design of optimum patch shape and size for bonded repair on damaged Carbon fibre reinforced polymer panels", *Mater. Des.*, **54**, 174-183.

Kumar, M.A. and Hakeem, S.A. (2000), "Optimum design of symmetric composite patch repair to centre cracked metallic sheet", *Compos. Struct.*, **49**, 285-292.

Mhamdia, R., Serier, B., Bachir Bouiadjra, B. and Belhouari, M. (2012), "Numerical analysis of the patch shape effects on the performances of bonded composite repair in aircraft structures", *Compos. Part B*, **43**, 391-397.

Mokadem, S., Bachir Bouiadjra, B., Mechab, B. and Kaddouri, K. (2015), "Elastic-plastic analysis of the J integral for repaired cracks in plates", *Adv. Mater. Res.*, **4**(2), 87-96.

Neapolitan, R.E. (2004), *Learning Bayesian Networks*, Pearson Prentice Hall.

Papanikos, P., Tserpes, K.I. and Pantelakis, S. (2007), "Initiation and progression of composite patch debonding in adhesively repaired cracked metallic sheets", *Compos. Struct.*, **81**, 303-311.
Ramji, M., Srilakshmi, R. and Prakash, M.B. (2013), "Towards optimization of patch shape on the performance of bonded composite repair using FEM", *Compos. Part B*, **45**, 710-720.
Shiuh-Chuan, H. and Chao, M. (2011), "Adhesively bonded patch repair of composite laminates", *J. Adhes. Sci. Tech.*, **25**(18), 2569-2585.
Tsai, G. and Shen, S.B. (2004), "Fatigue analysis of cracked thick aluminum plate bonded with composite patches", *Compos. Struct*., **4**, 79-90.

CC